Research Square

Preprints are preliminary reports that have not undergone peer review.
They should not be considered conclusive, used to inform clinical practice,
or referenced by the media as validated information.

Improving Radar Rainfall Estimate with Kalman Filter Based Bias Adjustment Methods

Feiyang Lv
Nanjing University of Information Science and Technology
Alan Seed
Weather Radar New Zealand Limited
Yong Wang
yong.wang@nuist.edu.cn

Earth System Modeling and Prediction Centre

Short Report

Keywords: Radar rainfall estimation, Kalman filter, Bias correction, Optical flow

Posted Date: March 18th, 2026

DOI: https://doi.org/10.21203/rs.3.rs-9046179/v1

License: This work is licensed under a Creative Commons Attribution 4.0 International License.
Read Full License

Additional Declarations: No competing interests reported.

Improving Radar Rainfall Estimate with Kalman Filter Based Bias Adjustment Methods

Feiyang Lv[1]

Alan Seed[2]

Yong Wang[1,3,4*]

Correspondence: yong.wang@nuist.edu.cn

Author details

1 School of Atmospheric Sciences, Nanjing University of Information Science and Technology, 219 Ningliu Road, Pukou District, Nanjing, Jiangsu, 210044, China

2 Visiting Professor at NUIST, and Weather Radar New Zealand Limited, 101 Pakenham Street West, Auckland Central, Auckland, 1010, New Zealand.

3 Earth System Modeling and Prediction Centre, China Meteorological Administration, Beijing, 100081, China.

4 State Key Laboratory of Severe Weather Meteorological Science and Technology, Beijing, 100080, China.

Abstract

This study evaluates three real-time Kalman filter (KF) approaches—Mean Field (MKF),

Site-Specific (SKF), and a novel Lagrangian (LKF)—to correct radar rainfall estimation biases. While the SKF addresses spatial heterogeneity by applying independent filters per gauge, the LKF uniquely utilizes optical flow to advect the bias correction field alongside moving storms. This prevents the erroneous spatial propagation of large correction factors into trailing light rain areas. Evaluated using a dense gauge network in northern China, the LKF demonstrates superior performance, reducing the raw radar's systemic bias from -35.0% to -3.5% while minimizing overall errors. However, these performance improvements diminish rapidly beyond a 10 km distance from the training gauges. Furthermore, an analysis of optimized filter parameters reveals a fundamental physical constraint: the KF breaks down when radar measurement variance (S) exceeds the intrinsic process variance (Q). Because these errors are independent, the filter remains effective only when the observed residual variance is less than 2Q. This demonstrates that dynamic algorithmic corrections cannot compensate for fundamentally degraded radar observations.

Keywords

Radar rainfall estimation, Kalman filter, Bias correction, Optical flow

Statements and Declarations

Competing interests

The authors declare that they have no competing interests.

1 Introduction

Weather radars are uniquely able to provide high-resolution estimates of rainfall over large areas but the use of these data for applications such as flood warning is constrained by the presence of occasional large errors (Berne and Krajewski 2013). Variability in the Z–R relationship has long been recognized as a source of error in radar rainfall estimation, dating back to early work such as Zawadzki (1975), and was one of the motivations for developing dual-polarimetric radar technology (e.g., Ryzhkov and Zrnić 1995). However, fluctuations in the Z–R relationship are only one of many sources of uncertainty. Villarini and Krajewski (2010) identified nine contributing factors to errors in single-polarization radar rainfall estimates, including calibration issues, signal attenuation, ground clutter, beam blockage, vertical structure of precipitation, and temporal changes in the Z–R relationship. Borga et al. (2022) highlighted three key challenges: dynamic variations in the Z–R relationship, the complexity of the vertical reflectivity profile (VPR), and terrain-induced beam obstruction.

For a single-polarization radar, radar reflectivity measured aloft must be corrected for these systematic errors and projected to the surface, and a Z–R relationship must be used to estimate the rainfall rate. The simplest approach is to select a Z-R relationship that has been published in the literature, e.g. Marshall and Palmer (1948). The next level in complexity is to use different relationships for stratiform and convective rain for example (Lee and Zawadzki 2005, You et al. 2022) and to classify the rainfall fields in real-time. Real-time adjustments based on rain gauge observations is widely used to improve the quality of operational radar rainfall estimates. Review of radar adjustment and gauge-radar merging techniques can be found in Ochoa-Rodriquez et al. (2019). Gauge adjustment techniques generally assume a uniform adjustment e.g. (Goudenhoofdt 2009, Emmanuel 2012, Libertino et al. 2015, Imhoff et al. 2021) or local adjustment e.g. Seo and Breidenbach (2002).

Algorithms that use a Kalman filter to predict mean field bias have been employed for operational bias correction for several decades (Smith and Krajewski 1991; Anagnostou et al. 1998; Seo and Breidenbach 2002; Chumchean and Seed 2006). More recently, Kim and Yoo (2014) developed a dual Kalman filter that accounts, at least conceptually, for systematic transitions between different rainfall regimes, such as stratiform and convective precipitation. Although Kalman filter–based dynamic

correction techniques can improve overall accuracy by recursively updating bias estimates, the underlying assumption of a spatially uniform multiplicative bias correction becomes limiting in complex or heterogeneous rainfall situations. More critically, most existing methods apply static, grid-based corrections in an Eulerian framework—that is, at fixed spatial locations—without accounting for the movement of the precipitation system. Because convective storms typically produce rainfall at a given location for only a short duration, the filter has limited opportunities to adjust to biases arising from the underlying meteorological conditions. One way to overcome this limitation is to treat the bias as a property of the rain field itself, rather than of fixed locations. This perspective allows the gauge network to sample the evolving bias more effectively as the precipitation system moves across the domain.

In this study, we implement and compare three Kalman filter–based radar bias correction approaches with increasing levels of spatial specificity and physical realism. The Mean Field Kalman Filter (MKF) assumes a spatially uniform, domain-averaged bias that evolves in time, providing a computationally simple baseline. The Site-Specific Kalman Filter (SKF) estimates and updates a separate bias for each gauge location, capturing spatial heterogeneity in radar-gauge discrepancies. Finally, the Lagrangian Kalman Filter (LKF) represents a novel formulation in which the bias is treated as a

property of the precipitation system itself, advected along with the storm using velocity fields. This allows the filter to better track evolving bias structures under convective storm movement, addressing a key limitation of fixed-location Eulerian approaches.

These three approaches are designed to test the hypothesis that incorporating spatial dynamics or storm motion can significantly improve radar-gauge bias correction, especially under heterogeneous and fast-changing rainfall conditions. To assess their performance, we apply each method to high-resolution radar and gauge data from northern China and evaluate the results using statistical error metrics across different rainfall intensities and storm types.

2 Data and Method

2.1 Data

This study utilizes high-resolution weather radar and dense rain gauge observations collected over northern China from June to August 2022. As illustrated in Figure 1, the spatial scope is limited to a 150 km radius around the Beijing SA radar to minimize vertical profile uncertainties. To ensure independent evaluation, the gauge network was randomly partitioned into a 75% calibration set for parameter estimation and a 25% validation set for out-of-sample assessment. These two subsets are denoted by blue dots

and yellow triangles in Fig. 1, respectively. Detailed descriptions of the radar quality control, optical flow temporal interpolation, and data preprocessing procedures are provided in the Supplementary Material.

2.2 Model for Correction Factors

Assume a network on *N* rain gauges located at positions $x_{1,}x_2,\ldots,x_n$ where the observed 15-minute accumulations are denoted $R_g(x_i,t)$ and the radar rainfall estimates at the gauge locations are denoted $R_r(x_i,t)$. Following the approach of Ciach and Krajewski (1999), Ciach, Morrissey et al. (2000), Chumchean, Seed et al. (2006), and Berenguer and Zawadzki (2008), the true 15-min rainfall accumulation for at a location x_i and time t, denoted $R(x_i,t)$, is assumed to be related to the radar derived estimate through a multiplicative correction a factor:

$$R(x_i,t) = \alpha(x_i,t)R_r(x_i,t), \quad (1)$$

Here $\alpha(x_i,t)$ is a random variable that accounts for the errors in the radar rainfall estimates. These errors are primarily attributed to fluctuations in the Z–R relationship, but they also include residual errors from quality control and vertical profile correction procedures, as well as sampling errors due to projecting volumetric radar observations onto a surface point.

Following Smith and Krajewski (1991), the correction factor $\alpha(x_i,t)$ is assumed to

126 follow a lognormal distribution. Define the logarithmic residual $y(x_i, t)$ as:

127 $$y(x_i, t) = \ln R_g(x_i, t) - \ln R_r(x_i, t)\,, \quad (2)$$

128 The correction factor y is undefined when either R_g or R_r is zero, and it becomes
129 highly unstable when either value is close to zero. This instability is relatively frequent
130 and arises from sources of random error in the measurement of $\alpha(x_i, t)$, such the
131 advection of the rain drops in the wind between the radar observations aloft and the rain
132 gauge at the surface (Lack and Fox 2005) and the mismatch between the sampling volume
133 of the radar and the rain gauge (Habib, Ciach et al. 2004). Therefore, $y(x_i, t)$ is
134 considered a valid observation when both R_g and R_r exceed 0.25 mm and the absolute
135 residual satisfies:

136 $$|y(x_i, t)| < 3 \quad (3)$$

137 Otherwise, $y(x_i, t)$ is excluded from the analysis.

138 If the spatiotemporal variation of the correction factors is assumed to consist of
139 random fluctuations about a mean value plus a measurement error, then the observed
140 correction factor can be expressed as:

141 $$\mathrm{y}(x_i, t) = \alpha(x_i, t) + v(x_i, t) + \mu(x_i) \quad (4)$$

142 Here α is a random variable $\alpha(x_i) \sim \mathcal{N}(0, \sigma_\alpha^2)$ that represents the random fluctuations
143 of the correction factors about the expected value at location x_i, $\mu(x_i)$, and v is a random

variable that represents the measurement error. $\mu(x_i)$ reflects both the bias arising from the use of a fixed Z–R relationship and any systematic errors associated with the radar rainfall estimation algorithms at that location, for example partial occultation.

2.3 Kalman filter model

Following Kalman (1960), and in order to facilitate a comparison of the similarities and differences between the proposed methods, we transform the equation of the generalized Kalman filter into a more intuitive standard one-dimensional Kalman filter framework. The prediction step is written as:

$$x_{k|k-1} = \phi x_{k-1|k-1}, \tag{5}$$

$$P_{k|k-1} = \phi^2 P_{k-1|k-1} + (1-\phi^2)Q, \tag{6}$$

Where $x_{k|k-1}$ is the predicted estimate of the state at time k, given data at time k-1, ϕ is the state transition coefficient, i.e., the autoregressive coefficient. $P_{k|k-1}$ represents the prediction error covariance, used to quantify the uncertainty of the prior state estimate at time k. Its calculation is based on the error covariance $P_{k-1|k-1}$ of the previous time step, transmitted through the system dynamics process, and supplemented by the process noise covariance Q, which characterizes the uncertainty introduced by the model itself.

$$K_k = \frac{P_{k|k-1}}{P_{k|k-1} + S} \tag{7}$$

$$x_{k|k} = x_{k|k-1} + K_k\left(y_k - x_{k|k-1}\right) \tag{8}$$

$$P_{k|k} = (I - K_k)P_{k|k-1} \tag{9}$$

Where S is the variance of the measurement error and $x_{k|k}$ is the updated estimate based on the new observation y_k.

The filter is initialised by setting:

$$x_{0|0} = 0 \tag{10}$$

$$P_{0|0} = \sigma_\alpha^2 \tag{11}$$

If the observed correction factor is undefined at t, then set:

$$x_{k|k} = x_{k|k-1} \tag{12}$$

$$P_{k|k} = P_{k|k-1} \tag{13}$$

2.3.1 Mean Field Kalman Filter algorithm

MKF assumes that the deviation across the entire radar coverage area is spatially uniform. where the state definition in Eq. (5) is:

$$x_k = \beta_k \tag{14}$$

Where β_k is the logarithmic deviation of the overall average.

The prediction step changes as follows:

$$\beta_{k|k-1} = \phi\beta_{k-1|k-1} \tag{15}$$

2.3.2 Site Specific Kalman Filter algorithm

Under the SKF framework, we assume that radar bias is spatially non-uniform and

captures local features by running a filter independently for each rain gauge station i, where the state definition in Eq. (5) is:

$$x_k = \alpha(x_i, t) \tag{16}$$

The prediction step changes as follows:

$$\alpha(x_i, t|t-1) = \phi\alpha(x_i, t-1|t-1) \tag{17}$$

2.3.3 Lagrangian Kalman Filter algorithm

SKF operates on a single-point time series, ignoring information that can be obtained from the spatial structure of the correction field. Since the correction factor depends on meteorological processes, it is reasonable to consider it as a precipitation field attribute that moves with the weather system within the region, rather than an attribute specific to a particular geographic location within that region. Based on this, we propose LKF. This method treats the correction factor y as a field transported by advection within the region, thereby increasing the amount of observational data available for estimating the true state. Assuming that the evolution of the correction field is sufficiently slow between observations, we can set:

$$\frac{\partial \alpha}{\partial t} + \mathbf{v} \cdot \nabla \alpha = 0 \tag{18}$$

Where $\mathbf{v}$ is the apparent velocity field estimated by the optical flow method (Horn and Schunck, 1981), and here the bias field $\alpha(x, t)$ is a property of the precipitation cloud

itself, rather than a property of a fixed geographical location. We define the state in Eq. (5) as:

$$x_k = \alpha(x, t) \tag{19}$$

The prediction step changes as follows:

$$\alpha(x, t|t-1) = \phi\alpha(x - \mathbf{U}(x)dt, t-1|t-1) \tag{20}$$

Where x is a set of regular grid points covering the entire region with a spatial resolution of 1 km; $\mathbf{U}(x)$ is the apparent velocity field, which is calculated and updated using $\alpha(x, t)$ and $\alpha(x, t-1)$ through an optical flow algorithm. For all three frameworks (MKF, SKF, and LKF), the update step follows the standard form described in Eq. (7-9), where the predicted state is adjusted by the latest valid gauge observation weighted by the Kalman gain.

2.3.4 Parameter estimation

The Kalman filter framework relies on three core parameters: the autoregressive coefficient, process noise variance, and measurement error variance. We independently optimized these parameters for each rain gauge using the Nelder-Mead algorithm to minimize the first-order autocorrelation of the residual sequence. To mitigate the equifinality problem and ensure physical relevance, strict boundary constraints were

imposed during optimization. (detailed in the Supplementary Material)

2.4 Evaluation Metrics

The performance was independently assessed using the 25% validation gauge dataset. Three statistical metrics were employed: Mean Absolute Error (MAE), Root Mean Square Error (RMSE), and Percentage Bias.

3 Results

3.1 Parameter Relationship Analysis

A common critique of multiparameter filtering is equifinality, where different parameter combinations yield similar performance. To address this, we examined the phase space dependence among the optimized SKF parameters (Fig. 2). The results reveal a strong, physically meaningful coupling rather than random mathematical artifacts. Gauges with lower measurement uncertainty ($S < 0.08$) consistently exhibit higher ϕ and Q values. This indicates that when radar observations are relatively clean, the filter confidently assigns higher memory and process variance to track the true evolution of the Z–R relationship. Conversely, when measurement noise dominates ($S > 0.11$, typically located at the edge of the radar scan or in mountainous regions), the signal from the underlying microphysical process is obscured. Crucially, the filter breaks down when the

measurement variance (S) exceeds the process variance (Q). Because the process and measurement errors are statistically independent, the total variance of the observed residuals is the sum of S and Q.

Supplementary Fig. S1 shows the spatial distributions and probability density functions of the SKF parameters. The autoregressive coefficient ϕ is lower near Beijing but higher in peripheral areas. Measurement variance S is markedly higher at the radar edges and mountainous regions due to beam broadening and blockage, while process variance Q remains relatively uniform. The PDFs indicate mean values of 0.694 (ϕ), 0.111 (Q), and 0.080 (S). These patterns demonstrate that local radar data quality strongly influences Kalman filter parameters.

Therefore, for the filter to remain effective and extract meaningful signals, the variance of the observed residuals must be less than $2Q$. When this threshold is exceeded, the filter intelligently reduces ϕ and Q, leading to highly conservative updates. This demonstrates the robustness of the parameter estimation algorithm and highlights that algorithmic correction cannot compensate for fundamentally degraded radar observations.

3.2 Performance Evaluation of Kalman Filter–Based Correction Methods

The performance of the MKF, SKF, and LKF methods was evaluated exclusively at the 25% independent validation gauges. Table 1 summarizes the overall error metrics.

The raw radar exhibits a severe systemic underestimation, with a bias of -34.99%. While the MKF slightly reduces this bias, the LKF achieves the best overall performance, minimizing both the MAE and RMSE, and effectively eliminating the systemic bias. Interestingly, the SKF overcompensates, resulting in an overall positive bias and inflated RMSE. In the Fig. 3, the probability density functions of the estimation residuals further illustrate this: while the SKF and LKF produce sharper peaks near zero compared to the raw radar, the SKF's residual distribution exhibits a noticeable positive skew.

3.3 Spatial Dependence of Error Metrics

To address the spatial dependency of the correction methods, Fig. 4 presents the error metrics as a function of the distance to the nearest training gauge, supported by the observation counts in Table S1. The vast majority of the validation observations are located within 2–8 km from a training gauge. At close ranges, the SKF and LKF demonstrate substantial reductions in bias compared to the raw radar. However, this benefit diminishes with increasing distance. Beyond 10 km, the performance of the KF methods gradually converges. This highlights that the proposed KF frameworks function fundamentally as gauge-enhanced radar products. While the LKF maintains a more stable bias profile at larger distances, neither method can meaningfully extend the spatial influence of gauge information beyond the typical spatial decorrelation distance of

localized convective storms.

3.4 Error Characteristics across Rainfall Intensities

As shown in Fig. 5 and Table S2, the performance disparities among the methods are strongly linked to rainfall intensity. For heavy precipitation events exceeding 30 mm/h, the raw radar severely underestimates rainfall. Both the SKF and LKF successfully correct this underestimation. However, in the light rainfall category of 0 to 5 mm/h, which constitutes the largest sample size of 20,483 observations, the SKF suffers from severe "over-correction," leading to the overall positive bias observed in Table 1. This occurs because large correction factors generated in heavy convective cores are erroneously propagated to adjacent light-rain areas via spatial interpolation. Crucially, the LKF effectively mitigates this over-correction. By tracking storm motion via optical flow, the LKF advects the high-magnitude correction factors along with the convective cores, significantly reducing the spurious amplification of light rainfall while preserving the correction accuracy in heavy rainfall.

To explicitly demonstrate the physical efficacy of this Lagrangian framework, Fig. 6 illustrates the temporal evolution of the LKF spatial correction factor α during a severe convective event on June 12, 2022. Between 18:40 and 19:40, a high-magnitude adjustment core indicated by the red cluster with α values exceeding 1.5 can be clearly

observed advecting southeastward. In a Eulerian framework like MKF or SKF, these extreme correction factors would decay in place, erroneously amplifying trailing light rainfall after the convective core has moved away. In contrast, the visual evidence confirms that the LKF successfully uses optical flow to advect the correction field alongside the storm cell. By moving the extreme bias correction factors along the storm's trajectory, the LKF preserves the spatial representativeness of the correction and minimizes false alarms in post-storm regions.

4 Discussion

This study proposed and evaluated three real-time bias correction frameworks for radar rainfall estimation. By rigorously separating calibration and validation datasets, we demonstrated that dynamic correction mechanisms, particularly the LKF, significantly outperform static Z–R relationships.

The introduction of the LKF represents a conceptual advancement by treating the bias as a property of the moving precipitation system rather than a fixed geographic location. As demonstrated across varying rainfall intensities, the Lagrangian approach successfully mitigates the over-correction problem associated with traditional Eulerian spatial interpolations in light rain, yielding the lowest overall RMSE and MAE.

However, the Lagrangian assumption has inherent limitations. The LKF relies on

optical flow to advect the correction field (Eq. 18), intentionally neglecting microphysical source/sink terms. During rapidly evolving convective events—where storms initiate or dissipate abruptly—this pure advection assumption is violated. The optical flow may propagate historical large correction factors into regions where the storm has already decayed, yielding localized over-corrections. Furthermore, the rapid degradation of performance beyond 8–10 km underscores that real-time correction algorithms cannot fully compensate for sparse gauge networks or fundamentally degraded radar observations.

In conclusion, while the SKF provides strong local bias correction, the LKF offers a physically intuitive alternative that suppresses spatial over-correction. Future research should focus on integrating microphysical source/sink dynamics into the Lagrangian framework to further stabilize radar rainfall estimation under explosive convective conditions.

Acknowledgements

The authors gratefully acknowledge the CMA for providing the radar and rain gauge data used in this study. We also thank our colleagues at the Hebei Provincial Meteorological Bureau for their assistance. The first author would like to express his

sincere gratitude to Prof. Alan Seed for his invaluable guidance, continuous support, and insightful physical interpretations throughout this research and the revision process.

Author Contributions

Feiyang Lv conceptualized the study, developed the Lagrangian Kalman filter framework, performed data analysis, optimized Kalman filter parameters, prepared figures and tables, and wrote the original draft of the manuscript.

Alan.Seed provided critical guidance on Kalman filter theory, optical flow application, and bias correction methodologies, contributed to the physical interpretation of results, and revised the manuscript for important intellectual content.

Yong.Wang supervised the overall research, secured data access from CMA, contributed to the design of the experimental setup, validated the results, and critically reviewed and edited the manuscript.

All authors read and approved the final version of the manuscript and agree to be accountable for all aspects of the work.

Data Availability

The radar and rain gauge datasets analyzed during the current study are not publicly

available due to the strict data access policies of the China Meteorological Administration (CMA), but they are available from the corresponding author on reasonable request and subject to necessary institutional approvals.

References

Anagnostou EN, Krajewski WF, Seo D-J, Johnson ER (1998) Mean-field rainfall bias studies for WSR-88D. J Hydrol Eng 3:149–159.

Berenguer M, Zawadzki I (2008) A study of the error covariance matrix of radar rainfall estimates in stratiform rain. Wea Forecasting 23:1085–1101. doi:10.1175/2008WAF2222134.1.

Berne A, Krajewski WF (2013) Radar for hydrology: Unfulfilled promise or unrecognized potential? Adv Water Resour 51:357–366. doi:10.1016/j.advwatres.2012.05.005. Borga M, Marra F, Gabella M (2022) Rainfall estimation by weather radar. In: Morbidelli R (ed) Rainfall. Elsevier, 109–134.

Chumchean S, Seed A, Sharma A (2006) Correcting of real-time radar rainfall bias using a Kalman filtering approach. J Hydrol 317:123–137. doi:10.1016/j.jhydrol.2005.05.019.

Chumchean S, Sharma A, Seed A (2006) An integrated approach to error correction for

real-time radar-rainfall estimation. J Atmos Oceanic Technol 23:67–79. doi:10.1175/JTECH1832.1.

Ciach GJ, Krajewski WF (1999) Radar–rain gauge comparisons under observationnal uncertainties. J Appl Meteor 38:1519–1525. doi:10.1175/1520-0450(1999)0382.0.CO;2.

Ciach GJ, Morrissey ML, Krajewski WF (2000) Conditional bias in radar rainfall estimation. J Appl Meteor 39:1941–1946. doi:10.1175/1520-0450(2000)0392.0.CO;2.

Emmanuel I, Andrieu H, Tabary P (2012) Evaluation of the new French operational weather radar product for the field of urban hydrology. Atmos Res 103:20–32. doi:10.1016/j.atmosres.2011.06.013. Goudenhoofdt E, Delobbe L (2009) Evaluation of radar-gauge merging methods for quantitative precipitation estimates. Hydrol Earth Syst Sci 13:195–203. doi:10.5194/hess-13-195-2009.

Habib E, Ciach GJ, Krajewski WF (2004) A method for filtering out raingauge representativeness errors from the verification distributions of radar and rain-gauge rainfall. Adv Water Resour 27:967–980. doi:10.1016/j.advwatres.2004.05.001.

Horn, B. K., & Schunck, B. G. (1981). Determining optical flow. Artificial intelligence, 17(1-3), 185-203. doi.org/10.1016/0004-3702(81)90024-2.

377 Imhoff R, Brauer C, van Heeringen KJ, Leijnse H, Overeem A, Weerts A, Uijlenhoet R
378 (2021) A climatological benchmark for operational radar rainfall bias reduction.
379 Hydrol Earth Syst Sci 25:4061–4080. doi:10.5194/hess-25-4061-2021.
380 Kalman RE (1960) A new approach to linear filtering and prediction problems. J Basic
381 Eng 82:35–45. doi:10.1115/1.3662552.
382 Kim J, Yoo C (2014) Use of a dual Kalman filter for real-time correction of mean field
383 bias of radar rain rate. J Hydrol 519:2785–2796. doi:10.1016/j.jhydrol.2014.09.040.
384 Lack SA, Fox NI (2005) Errors in surface rainfall rates retrieved from radar due to wind-
385 drift. Atmos Sci Lett 6:71–77. doi:10.1002/asl.98.
386 Lee GW, Zawadzki I (2005) Variability of drop size distributions: Time-scale dependence
387 of the variability and its effects on rain estimation. J Appl Meteor 44:241–255.
388 doi:10.1175/JAM2183.1.
389 Libertino A, Allamano P, Claps P, Cremonini R, Laio F (2015) Radar estimation of intense
390 rainfall rates through adaptive calibration of the Z-R relation. Atmosphere 6:1559–
391 1577. doi:10.3390/atmos6101559.
392 Marshall JS, Palmer WMK (1948) The distribution of raindrops with size. J Atmos Sci
393 5:165–166. doi:10.1175/1520-0469(1948)0052.0.CO;2.
394 Ochoa-Rodriguez S, Wang L-P, Willems P, Onof C (2019) A review of radar-rain gauge

data merging methods and their potential for urban hydrological applications. Water Resour Res 55:6356–6391. doi:10.1029/2018WR023332.

Ryzhkov AV, Zrnić DS (1995) Comparison of dual-polarization radar estimators of rain. J Atmos Oceanic Technol 12:249–256. doi:10.1175/1520-0426(1995)0122.0.CO;2.

Seo D-J, Breidenbach JP (2002) Real-time correction of spatially nonuniform bias in radar rainfall data using rain gauge measurements. J Hydrometeor 3:93–111. doi:10.1175/1525-7541(2002)0032.0.CO;2.

Smith JA, Krajewski WF (1991) Estimation of the mean field bias of radar rainfall estimates. J Appl Meteor 30:397–412. doi:10.1175/1520-0450(1991)0302.0.CO;2.

Villarini G, Krajewski WF (2010) Review of the different sources of uncertainty in single polarization radar-based estimates of rainfall. Surv Geophys 31:107–129. doi:10.1007/s10712-009-9079-x.

You C-H, Kim H-J, Suh S-H, Jung W, Kang M-Y (2022) The characteristics of raindrop size distributions in different climatological regions in South Korea. Remote Sens 14:5137. doi:10.3390/rs14205137.

Zawadzki I (1975) On radar-raingauge comparison. J Appl Meteor 14:1430–1436. doi:10.1175/1520-0450(1975)0142.0.CO;2.

Figure Legends

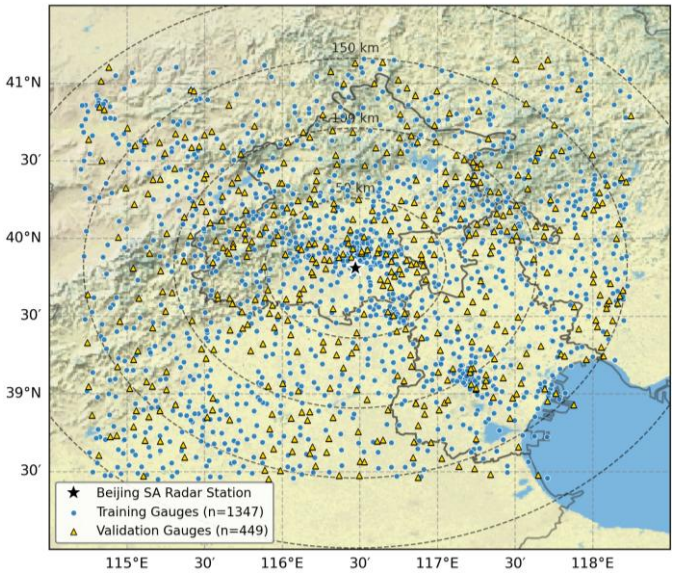


Fig. 1 Spatial configuration of the study area, topography, and the rain gauge network. The Beijing SA radar is denoted by a black star, surrounded by 50, 100 and 150km range rings. Blue dots and yellow triangles represent the training (75%) and validation (25%) gauge stations, respectively.

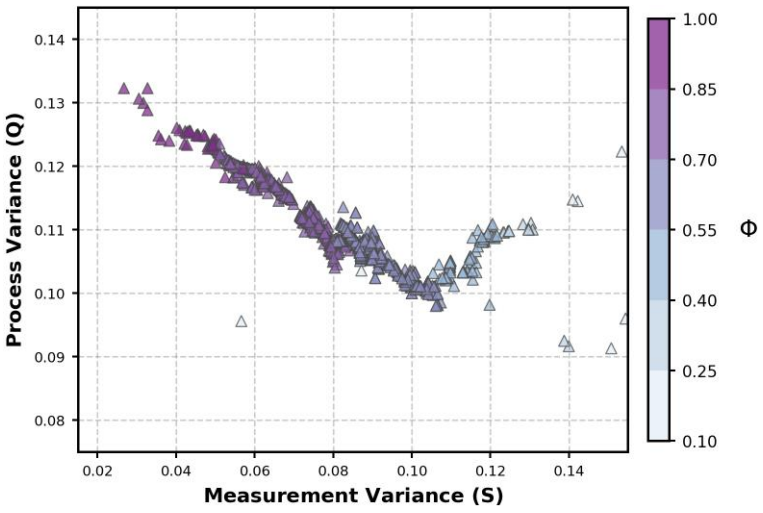


Fig. 2 Phase space dependence among the optimized Kalman filter parameters. The scatter plot illustrates the coupling relationship between the measurement variance (S) and the process variance (Q), with colors representing the magnitude of the autoregressive coefficient (ϕ).

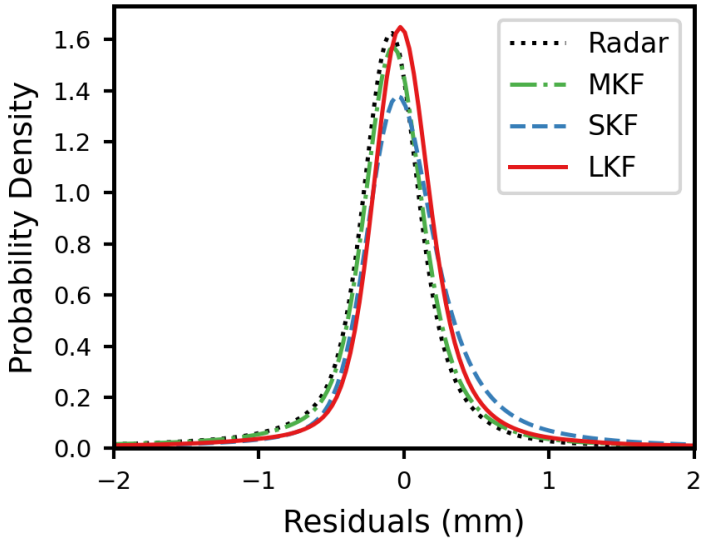
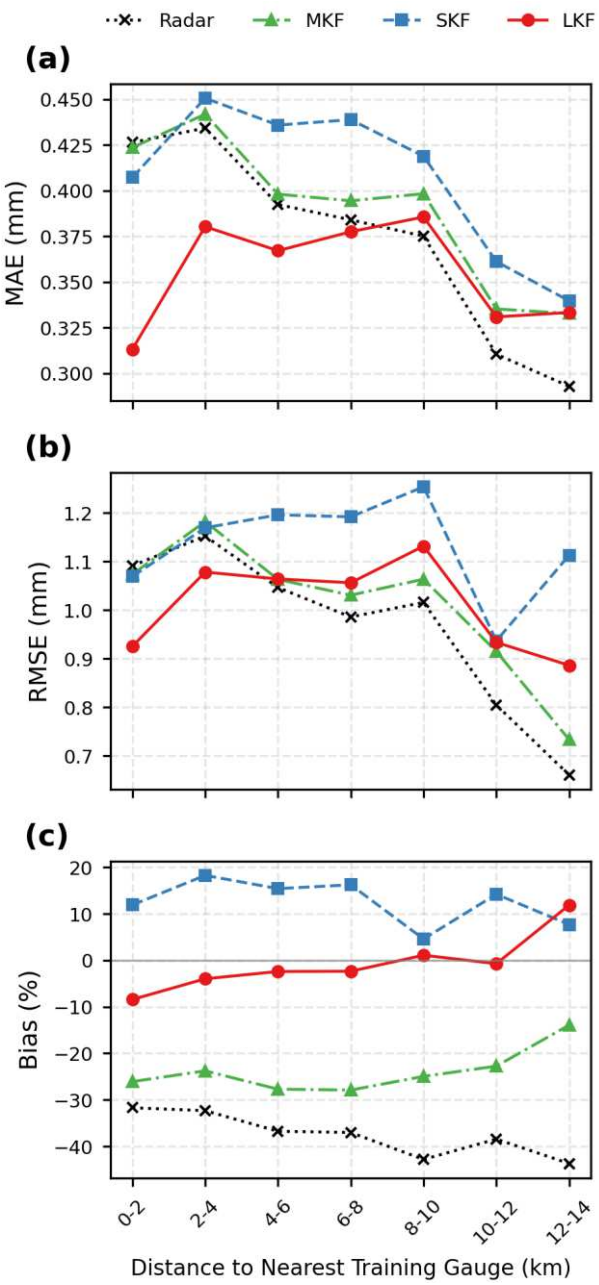


Fig. 3 Probability density functions of the rainfall estimation residuals (estimated minus observed) for the raw radar,MKF, SKF, and LKF evaluated on the validation set.



428

429 **Fig. 4** Performance evaluation metrics, including (a) MAE, (b) RMSE, and (c) Bias, for

430 the raw radar and three adjustment methods (MKF, SKF, LKF) as a function of the

431 distance to the nearest training gauge.

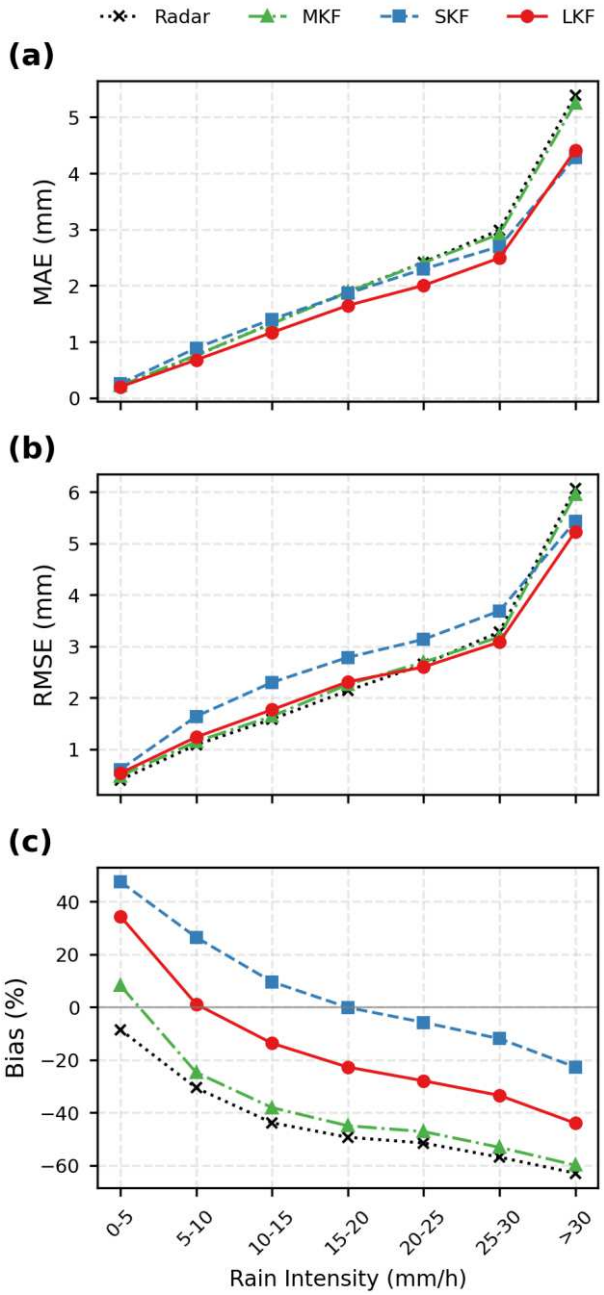
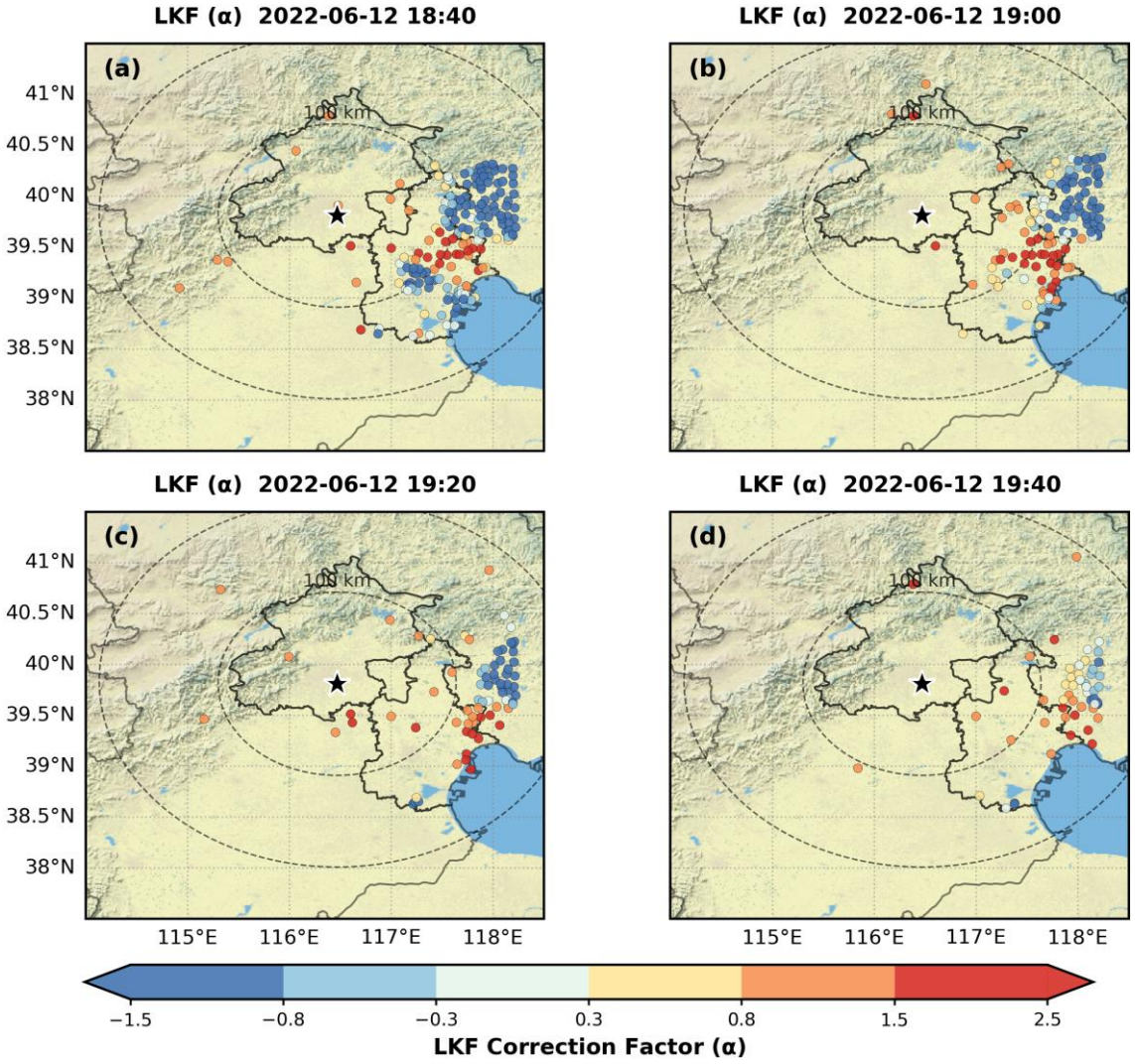


Fig. 5 Performance evaluation metrics, including (a) MAE, (b) RMSE, and (c) Bias, for the raw radar and three adjustment methods (MKF, SKF, LKF) under different rainfall intensity categories. The horizontal solid line in (c) denotes the zero-bias reference.



436

437 **Fig. 6** Spatial and temporal evolution of the LKF correction factor (α) from 18:40 to

438 19:40 LST on June 12, 2022. The panels demonstrate the advection of the bias

439 correction field along the storm trajectory.

Tables

Table 1: Overall performance of the rainfall estimation methods evaluated on the independent validation set.

Method	RMSE (mm)	MAE (mm)	Bias (%)
Radar	1.071	0.406	-34.993
MKF	1.094	0.413	-26.039
SKF	1.172	0.435	15.526
LKF	1.052	0.366	-3.492

Supplementary Files

This is a list of supplementary files associated with this preprint. Click to download.

- solasupply.docx